Beam tilt and angular dispersion in broad-bandwidth, nanosecond optical parametric oscillators

W. J. Alford, Russell J. Gehr, R. L. Schmitt, and A. V. Smith

Dept. 1128 Lasers, Optics and Remote Sensing, Sandia National Laboratories, Albuquerque, NM 87185-1423

Gunnar Arisholm

Forsvarets forskningsinstitutt (Norwegian Defence Research Establishment) PO Box 25, N-2007 Kjeller, Norway

Abstract

We show that the signal and idler beams generated by certain types of unseeded, nanosecond optical parametric oscillators are tilted and angularly dispersed and have anomalously large bandwidths. This effect is demonstrated in both laboratory measurements and a numerical model. We show how the optical cavity design influences the tilts and how they can be eliminated or minimized. We also determine the conditions necessary to injection seed these parametric oscillators.

1. Introduction

Critically phase matched parametric mixing in nonlinear crystals achieves phase matching by counteracting refractive index dispersion with crystal birefringence. It always involves both extraordinary (e) and ordinary (o) polarizations. As is well known, e-polarized waves undergo birefringent walk-off, meaning their Poynting vectors are tilted relative to their propagation vectors by a walk-off angle ρ. These tilts break the reflection symmetry in the walk-off plane, permitting the development of beam tilts in the mixing process[1]. This admits

DISCLAIMER

DISCLAIMER

Portions of this document may be illegible in electronic image products. Images are produced from the best available original document.

the possibility that the beams generated in a critically phase matched optical parametric oscillator (OPO) might be tilted relative to the axis of the optical cavity. A number of variables might be expected to influence such tilts, including the optical cavity design, the pump beam diameter, the walk-off angles, whether the resonated wave is an *e* or an *o* wave, and the degree of phase mismatch. Another well known feature of critically phase matched nonlinear mixing is that the phase matching angle depends on the wavelengths. This could lead to angular dispersion of the signal and idler wavelengths generated in a broad bandwidth, critically phase matched OPO. For example, if a monochromatic pump wave is aligned along the cavity axis of a standing wave, type II (signal and idler orthogonally polarized) OPO, only one signal frequency will phase match along this axis. If the signal frequency deviates slightly from this value, the phase matching angle shifts slightly, perhaps leading to angular dispersion of the output wavelengths. The degree of dispersion would depend primarily on the phase matching properties of the crystal but most likely would also be influenced by the same design parameters as the tilt.

Signal beam tilts have been reported by Haub *et al.*[2] for a type II KTP OPO, and dispersion has been noted in a type I BBO OPO[3]. In this paper we report observation of tilts and dispersion both in laboratory measurements of a broad-bandwidth, critically phase matched, standing-wave KTP OPO, and in a numerical model of it, with good agreement between them. We explain in some detail how tilts and dispersion develop based on an understanding gleaned from numerous computer simulations, and we discuss ways to eliminate or minimize them. We also examine the requirements for injection seeding OPO's in their presence. Where possible we support our model-derived conclusions with laboratory observations.

2. Numerical OPO model

Our numerical model for broad-bandwidth, nanosecond OPO's accounts for nonlinear mixing, diffraction, birefringent walk-off, group velocity, and group velocity dispersion of each

wave. It also incorporates a realistic model of quantum noise, including multiple transverse and longitudinal modes, permitting us to model unseeded or free running OPO's. The model numerically integrates three wave equations of the form[4]

$$\left[\frac{\partial}{\partial z} - \frac{i}{2k_j}\nabla_t^2 + \tan\rho_j\frac{\partial}{\partial x} + \frac{1}{v_j}\frac{\partial}{\partial t} + i\alpha_j\frac{\partial^2}{\partial t^2}\right]\varepsilon_j(x,y,z,t) = P_j(x,y,z,t)\exp(\pm i\Delta k z) \qquad (1)$$

where the ∇_t^2 term accounts for diffraction, the $\tan\rho_j$ term describes birefringent walk-off with angle ρ_j in the x direction, the v_j and α_j terms describe group velocity and group velocity dispersion respectively, and the P_j term is the driving polarization at frequency j, including primarily the second order nonlinear term but also linear absorption, nonlinear refractive index, and multiphoton absorption if they are of interest. The phase mismatch Δk is defined as $(k_p - k_s - k_i)$, and the plus sign in the exponential of Eq. (1) applies to the signal and idler equations while the negative sign applies for the pump equation. We use the split-step integration method in which linear propagation and nonlinear mixing are handled on alternating steps[5–8]. For the propagation half step over distance Δz, we Fourier transform the fields ε_j from $\{x,y,z,t\}$ space to $\{k_x,k_y,z,\omega\}$ space, shift the phase of each Fourier component as appropriate to account for diffraction, birefringent walk-off, group velocity, and group velocity dispersion, and then Fourier transform back to $\{x,y,z,t\}$ space. We then calculate the influence of the polarization term on ε_j over the same Δz step. Quantum noise at the signal and idler frequencies is incident on both mirrors from outside the cavity. This noise has a spectrum broader than the crystal's acceptance bandwidth, and is spatially structured to include more transverse modes than are supported by the OPO. In the cases described here, group velocity dispersion, nonlinear refractive index, and two photon absorption are expected to be unimportant and are not included. Typical execution times are a few hours on a 300 MHz Pentium II computer. To shorten execution time and reduce memory demands, we sometimes follow the development of only a fraction of a round-trip time slice as it circulates in the cavity[6,8]. This approximation will obviously not model all aspects of the OPO perfectly, but we find it gives a good approximation to the aspects of interest in this paper, namely conversion efficiency, pump thresholds, spectral

widths, beam tilts and angular dispersion.

Using this model we look first at the development of tilts. To focus on tilts without the added complexity of dispersion, we modeled monochromatic operation by limiting the injected noise to a single frequency while retaining its transverse spatial noise. The modeled device is the standing wave OPO diagrammed in Fig.1. It is pumped by a 10 ns, 532 nm pulse, and contains a KTP nonlinear crystal oriented for operation at signal and idler wavelengths of 784 nm and 1655 nm respectively. The pump and idler are *o* polarized and only the *e*-polarized signal wave is resonated. Birefringent signal walk-off in the 10 mm long crystal is 0.487 mm, comparable with the pump beam diameter of 0.65 mm. The physical cavity length is 12 mm. We begin with the KTP crystal aligned for exact phase matching with all beams parallel to the cavity axis. Throughout this discussion we define the phase mismatch Δk as that associated with this colinear geometry. With the mirror reflectivities set to zero for all waves, we first look at single pass behavior, and find the amplified signal and idler beams exiting the crystal are tilted by a few μrad, with the signal bent in the direction opposite walk-off and the idler bent toward walk-off. This we attribute to gain guiding, a reflection of the fact that parametric gain is highest for signal light that best maintains spatial overlap with the pump and idler beams. When the mirror signal reflectivities are set to 1.0 and 0.71, this gain-induced tilt causes the signal light to initially follow the course diagrammed in Fig. 2a. Over many cavity round trips the signal beam moves to the antiwalk-off side of the pump beam and stabilizes there. At threshold, loosely defined as the point where the pump is significantly depleted, we find that at the crystal exit face both the signal and idler beams are offset to the antiwalk-off side of the pump beam by about half the pump diameter. This initial offset of the signal beam suggests that a small tilt of the crystal might tilt the phase matching direction toward walk-off ($\Delta k < 0$) and this might counteract the gain-induced tilt, reducing the signal offset and giving better beam overlap. We tried a range of Δk's (or equivalently crystal tilts) with multitransverse mode (but still monochromatic) injected signal light, and found the gain and conversion efficiency were maximum for negative values Δk. Gain was nearly constant over the range

-19 < ΔkL <-9.5 corresponding to tilts of the generated signal beam outside the OPO ranging from 2.3 to 4.5 mrad in the walk-off direction. This means a monochromatic beam experiences the highest gain and earliest threshold not when the signal beam is aligned with the cavity axis and the crystal is phase matched for the signal beam along this axis, but for the crystal tilted slightly in the walk-off direction. The path followed by the signal beam then is diagrammed in Fig. 2b. In these simulations we notice that even with the crystal tilted for highest gain, the initial pump depletion is still displaced to the antiwalk-off side, but by a smaller amount than before. As the pump power and gain diminish late in the pulse, gain guiding decreases and we find the zone of pump depletion gradually moves to the walk-off side, as would be expected for a signal beam with propagation vector tilted in that direction. We note the signal tilt is relatively constant during the pulse, and the idler tilts in the direction opposite the signal at an angle larger by about $(n_s\omega_s/n_i\omega_i)$ as expected for transverse phase matching.

We deduce from this monochromatic modeling exercise that a given cavity design can have maximal gain at a nonzero phase mismatch. For different signal wavelengths this optimum value of Δk will occur at slightly different signal angles, of course, so for broad-bandwidth operation we might expect the signal wavelengths to be angle dispersed. In our OPO the bluer light will phase match better at larger tilts than the red light so dispersion is such that the blue is tilted further in the walk-off direction than the red. We find this is indeed the case when we initiate the model OPO with broad-bandwidth noise rather than with monochromatic noise, again keeping multiple transverse modes. Fig. 3 shows results of such a simulation of our test OPO pumped at twice threshold (6 mJ) illustrating both tilt and angular dispersion. The upper plot shows contours of signal fluence with beam tilt displayed on the horizontal axis, and offset from the phase matched frequency displayed on the vertical axis. The lower plot shows the corresponding far-field fluence contours. The point (0,0) in the upper plot corresponds to zero tilt relative to the cavity axis, and zero tuning from the frequency that is phase matched along the cavity axis. For our KTP crystal the variation of phase matching angle with signal frequency is calculated from the Sellmeier

equation[9] to be 3.41 μrad/GHz internal to the crystal or 6.19 μrad/GHz external assuming near-normal incidence on the exit face. This is the dashed line in the upper plot. The actual modeled dispersion is close to this value, but it is weakly influenced by cavity geometry leading to a smaller value of about 5.4 μrad/GHz.

3. Experiment

Our experimental setup is shown in figure 4. The 532 nm pump light is provided by frequency doubled output of a Q-switched, injection-seeded Nd:YAG laser in 10 ns, 12 mJ pulses. A variable attenuator and spatial filter/telescope condition the pump light before the OPO. The filter/telescope uses a 500 mm focusing lens, a 275 μm diameter pinhole, and a 200 mm collimating lens to create a near-Gaussian spatial profile beam of diameter 0.65 mm (FWHM), corresponding to a maximum fluence at the OPO of 2.5 J/cm^2. The 784 nm OPO seed light comes from a cw Ti:sapphire laser and has a maximum power of 20 mW. This beam is also spatially filtered and collimated to a diameter of 0.9 mm (FWHM). Both the pump and seed beams are incident on the OPO input mirror. Its reflectivities are 0.97 at 784 nm, 0.02 at 532 nm, and 0.18 at 1655 nm. The output coupler reflectivities are 0.72 at 784 nm, 0.008 at 532 nm, and 0.01 at 1655 nm. Our experimental procedure is to carefully align the pump and seed beams for colinear propagation and, with no mirrors installed, to adjust the crystal angle for maximum single-pass gain of the seed. This ensures that the crystal is aligned for zero phase mismatch in the direction of the beams. The OPO mirrors are then installed and adjusted to retroreflect the seed and pump, and to resonate the seed light with maximum finesse. The OPO cavity length is ramped by driving the PZT-mounted input mirror with a sawtooth voltage while the tilt of the output mirror is adjusted to maximize contrast of the cavity transmission resonance fringes. Cavity length is then locked to a transmission peak by small-amplitude dithering of the cavity length with a lock-in stabilizer (Lansing 80.215). This procedure ensures submilliradian alignment of the crystal and mirrors.

We characterize the OPO signal pulse with several measurements. To determine the angle between the signal and the pump beams, the beams are propagated 2 meters beyond the OPO and the maximum and minimum distances between the signal beam (which, for unseeded operation, spreads out considerably) and the pump spot are measured. The median value is used as the signal beam angle. The conversion efficiency of the OPO is measured by splitting off calibrated portions of the pump and signal beams for measurement by pyroelectric pulse energy meters (Laser Precision Rj-7200 Energy Ratiometers with RjP-735 heads). Their calibration is checked by comparison with calibrated laser calorimeters. Finally, for the measurement of signal beam angle versus wavelength (for unseeded operation) the signal beam is collimated in the direction orthogonal to walk-off (y-direction) by two cylindrical lenses and impinges on an 1800 lines-per-mm grating to disperse the wavelengths in the y direction. A 250 mm focal length lens focuses the negative-first order diffracted beam onto a video camera positioned 250 mm away, so beam tilt angle and wavelength correspond to image positions displaced along the x and y axes respectively. Far-field images of the signal beam are acquired using the same arrangement but with the cylindrical collimating lenses removed and with the grating replaced by a flat mirror.

4. Discussion

Representative dispersed and far-field energy flux contour images are shown in Figure 5 for the same pump level as in Figure 3 (6 mJ). Unlike the model results, these two profiles are for different pulses. Once again, the zero of the horizontal axis corresponds to the direction of the seed beam and the cavity axis, while the zero of the vertical axis corresponds to the frequency of the seed light. Note the absence of light at the seed frequency, a point we will discuss later. The measured dispersion of about 5.3 μrad/GHz is in good agreement with the model's value of 5.4 μrad/GHz. Note that the measured linewidth is also in fair agreement with the model predictions.

Given the good agreement between model and experiment, we feel justified in applying

the model to other OPO designs in order to draw useful conclusions about the behavior of various types of OPO's, and in particular to find ways to prevent tilts and dispersion. The most obvious peculiarities of our OPO are the broad bandwidths and frequency shifts of the signal and idler along with their large tilts and angular spreads. Furthermore, we find that for higher pump energies, both angular and frequency spreads increase, but the 5.3 μrad/GHz dispersion is constant. The measured bandwidth of 1000 to 2000 GHz is much greater than the OPO acceptance bandwidth (defined as the signal frequency detuning for which $\Delta kL{=}2\pi$) of 270 GHz. Our type II OPO behaves quite differently than type I OPO's which usually have bandwidths 2-5 times smaller than the acceptance bandwidth[3].

Based on our understanding of the evolution of tilt and dispersion gleaned from the monochromatic model, we might anticipate they could be avoided by using multiple walk-off compensating crystals in place of our single crystal. Gain guiding would tend to favor opposite tilts in the alternating crystals nulling the net tilt. Alternatively, we could use a single crystal in a ring cavity that reversed the tilt on alternate passes such as the three mirror ring we characterized in earlier work[7]. The plane of the ring lies in the walk-off plane so a tilt induced on one pass assumes the opposite sign on the next. Our model indicates that these designs do indeed avoid tilt and dispersion almost entirely. Table 1 summarizes model results for standing-wave and ring designs. The entry WOC-SW refers to the usual standing wave cavity with two walk-off compensating crystals, while ring refers to a single crystal in a three-mirror ring cavity with the same round-trip length. Both the walk-off compensating and ring designs eliminate tilts and dispersion and also narrow the linewidth. We have verified this in the laboratory using the same KTP crystal in a ring cavity and using two walk-off compensating 5 mm long KTP crystals in place of the 10 mm long KTP crystal in the usual standing wave cavity. The observed tilts are less than our measurement uncertainty of 0.5 mrad in both cases. Both model and experiment also indicate that double passing the pump beam in our standing-wave design nearly eliminates the signal and idler tilts. In this case, gain guiding on the return pass induces tilts opposite those created on the forward pass at least during the buildup to threshold. Additionally, the optimal value

of phase mismatch is zero so there is no wavelength shift in these designs.

Other entries in Table 1 refer to our usual standing wave OPO but with walk-off and cavity resonance assigned to different beams. Apart from being assigned to different waves, the walk-off angles and mirror reflectivities are kept constant. From the listed results, we conclude that it matters little whether the resonated beam is the one with walk-off or not. If either the signal or idler has walk-off there are tilts and detunings. However, the tilt of the resonated wave is nearly constant while the other has a tilt to preserve transverse phase matching, so resonating the redder wave results in smaller tilts and detunings. Tilt directions are such that the *e*-polarized beam tilts in the direction of walk-off. For the standing-wave, single-pump-pass design with no walk-offs on any beam (noncritical phase matching) there is no tilt or dispersion, and the linewidth of the signal and idler is substantially reduced. If walk-off is assigned to the pump rather than the signal or idler, as is appropriate for type I ($e \leftarrow oo$) phase matching, there are no tilts and the linewidth is about one quarter of the crystal's acceptance bandwidth as expected. The same is true for type I ($o \leftarrow ee$) phase matching.

If the beam path diagrammed in Fig. 2b is a valid explanation of signal tilts, lengthening the cavity while keeping crystal length constant should yield smaller tilts. We tested this in the laboratory by using a variety of cavity lengths and find that, as expected, tilts diminish with increasing cavity length. Our results are summarized in Table 2. Not surprisingly, we also find the threshold pump energy increases with cavity length. The variation of tilt with pump diameter more difficult to anticipate because gain guiding is influenced by both pump diameter and by the size of the signal and idler spatial structure. The model indicates that there is a slight increase in tilt and farfield angular spread with increasing pump diameter, but this trend is nearly buried in the pulse to pulse variations.

Earlier we gave an argument for the tilts and dispersion based on gain guiding and dispersion of the plane-wave phase matching angle. It is instructive to develop a complimentary description based on localized structure in the signal and idler beams that explains the dispersion in terms of temporal and spatial walk-off. For this it is convenient to express the

angular variation of phase matching angle with signal wavelength in terms of signal and idler group velocities and walk-off angles. We do this by assuming the contribution to Δk from a small signal tilt cancels that due to changes in signal frequency. That is $\Delta k_{\text{tilt}} = -\Delta k_{\text{tune}}$ for the noncolinear phase matching shown in Fig. 6. We calculate Δk_{tilt} for a pump beam tilted at angle θ_p relative to the optic axis z and with a small angle between the signal and idler k vectors. Keeping terms first order in $d\phi_s$, it is straightforward to show

$$\Delta k_{\text{tilt}} = \frac{2\pi n_s \nu_s}{c}(\rho_s + \phi_s - \rho_i + \phi_i)\,\delta\phi_s. \tag{2}$$

where we have used the relation between birefringent walk-off angle ρ and the refractive index

$$\rho_j = -\frac{1}{n_j}\frac{dn_j}{d\phi} \tag{3}$$

and assuming

$$\delta\phi_i = \frac{n_s \nu_s}{n_i \nu_i}\delta\phi_s. \tag{4}$$

Recalling that the Poynting vector of the signal beam, S_s, is at angle $(\alpha_s = \theta_p + \phi_s + \rho_s)$ and that of the idler is at angle $(\alpha_i = \theta_p - \phi_i + \rho_i)$, we rewrite this as

$$\Delta k_{\text{tilt}} = \frac{2\pi n_s \nu_s}{c}(\alpha_s - \alpha_i)\,\delta\phi_s. \tag{5}$$

The contribution to Δk from a signal frequency shift of $\delta\nu_s$ is

$$\Delta k_{\text{tune}} = \frac{2\pi}{c}(n_i + \frac{dn_i}{d\nu_i} - n_s - \frac{dn_s}{d\nu_s})\delta\nu_s \tag{6}$$

assuming $\delta\nu_s = -\delta\nu_i$. Using the definition of group velocity

$$\frac{1}{v_j} = \frac{1}{2\pi}\frac{dk_j}{d\nu_j} = \frac{1}{c}(n_j + \nu_j\frac{dn_j}{d\nu_j}) \tag{7}$$

this becomes

$$\Delta k_{\text{tune}} = \frac{2\pi}{c}(g_i - g_s)\delta\nu_s \tag{8}$$

where we have expressed the group velocity v_j in terms of a group velocity index g_j defined by $v_j = c/g_j$. The tilt and tune contributions to Δk cancel if

$$\frac{d\nu_s}{d\phi_s} = \frac{n_s \nu_s (\alpha_s - \alpha_i)}{g_s - g_i}. \tag{9}$$

Outside the crystal this dispersion becomes

$$\frac{d\nu_s}{d\phi_s} = \frac{\nu_s (\alpha_s - \alpha_i)}{g_s - g_i} \tag{10}$$

assuming small tilts of the exit face. Using the KTP values for group velocity indexes (1.875 and 1.765 for signal and idler respectively) and walk-off angle (47.5 and 0 mrad for signal and idler respectively) derived from the same Sellmeier equation[9] we find the same 3.41 μrad/GHz internal dispersion as before, corresponding to 6.19 μrad/GHz external.

This parameterization in terms of group velocity and Poynting vectors suggests an alternative description of dispersion in terms of slanted beam structure. Consider parametric amplification of a short, small diameter signal pulse by a longer, large diameter single-mode pump pulse as depicted on the left in Fig. 7a. Assuming an undepleted pump, we see that on exiting the crystal the signal and idler beams have the slanted envelopes diagrammed on the right in Fig. 7a, where the slant angle ϕ is given in terms of α_j and g_j by

$$\phi = \arctan\left[\frac{g_s - g_i}{\alpha_s - \alpha_i}\right]. \tag{11}$$

Such slanted pulses could equally well be formed by reflecting an unslanted pulse off a diffraction grating, as illustrated in Fig. 7b. Of course this reflection is associated with angular dispersion, and from the grating equation, the slant ϕ is easily related to the grating dispersion $d\phi/d\nu$ by

$$\phi = \arctan(\nu \frac{d\phi}{d\nu}) \tag{12}$$

implying by comparison of Eqs. (11) and (12) that the dispersion of the signal and idler light exiting the crystal can be expressed as

$$\frac{d\nu_s}{d\phi_s} = \frac{\nu_s (\alpha_s - \alpha_i)}{g_s - g_i}. \tag{13}$$

This is identical to Eq. (10), demonstrating the equivalence of descriptions in terms of phase matched plane waves or slanted envelopes. The latter description is usually invoked in analyzing parametric mixing where slanted pulses[10] are used to maintain short pulse durations and, by implication broad bandwidth, while the former is used to describe broad-bandwidth angle-compensated mixing[11]. This implies that if a mixing process creates slanted structure in the broad bandwidth signal and idler pulses in an OPO, there will be an angular dispersion given by Eqs. (10) and (13). Such slanted structure is almost inevitable given spatial and temporal modulation of the signal and idler beams combined with Poynting and group velocity walk-off. We have verified in detail these effects in a numerical model of single-pass parametric amplification[12].

It is clear from this understanding of the equivalence of slanted structure and dispersion that the important consideration in eliminating dispersion is that the signal and idler beams have colinear Poynting vectors so there is effectively no lateral walk-off and hence no slanted structure. This is automatically the situation for colinear type I mixing, but for our type II OPO noncolinear phase matching can accomplish this. If k_s is assumed to parallel the cavity axis, we can tilt the pump beam slightly to force k_i, and thus the idler Poynting vector, to parallel the signal Poynting vector at angle ρ_s. This requires the pump beam to be tilted in the walk-off direction by

$$\phi_p = \rho_s \frac{n_i \omega_i}{n_p \omega_p} = 15 \text{ mrad.} \tag{14}$$

There will be no slanted structures in this case and hence no dispersion. This is an example of tangential phase matching[13], the designation for noncolinear phase matching in which the Poynting vectors of an e and an o wave are parallel. According to Eq. (5) inducing a signal beam tilt via a phase mismatch when $\alpha_s = \alpha_i$ would require a very large value of Δk, but then the parametric gain would be severely reduced, so tilts are suppressed as well as dispersion. We verified this behavior in the laboratory. The OPO behaves much like a type I colinearly phase matched OPO. The treshold is minimized by tuning the crystal for zero phase mismatch, and there is no dispersion or tilt. The model produces the same result.

This method of eliminating tilts is convenient if the signal/idler tuning range is limited, but for large ranges the pump angle must be adjusted to maintain parallel Poynting vectors. Additionally, the idler will emerge with a large tilt so the other remedies discussed earlier may be more attractive in many applications.

Noncolinear pumping of type I OPO's is sometimes used to tune the OPO or to modify the acceptance bandwidth[14]. Because of the association of nonparallel signal and idler Poynting vectors with tilt and dispersion, we expect these devices will suffer the shortcomings of our standard OPO. Model runs verify this, predicting signal tilt, dispersion, and bandwidths proportional to the angle between the cavity axis and the pump propagation vector.

5. Injection seeding

We mentioned earlier that injection seeding was unsuccessful when the crystal was aligned for perfect phase match. In Fig. 5a we saw there was no signal light emitted at the seed frequency (zero frequency). However, if we rotate the crystal to shift the signal spectrum to the red (decrease θ) so its red end coincides with the injected signal frequency, partial seeding is possible, but only if the cavity length is locked to resonate the injected seed light. In Figure 8 we show the resulting far-field and dispersed images. There is a beam lobe associated with the seed light that has the same frequency as the seed but with a tilt of about 2 mrad relative to the seed and cavity axes. We find that to achieve robust seeding it is necessary to further tilt the crystal so its free running spectrum is centered on the seed frequency and also to tilt the seed beam so it is aligned with the median tilt of the free running seed. In this case one should be aware of frequency shifts on the order of the cavity free spectral range due to both Fabry-Perot resonance shift with beam tilt and to phase-mismatch-induced frequency shifts[15]. The OPO configurations that eliminate beam tilts, such as the three-mirror ring or the walk-off compensated standing-wave cavity, seed reliably with no such shifts or tilts.

6. Conclusions

We showed both in the laboratory and in numerical modeling that standing-wave, nanosecond OPO's with nonparallel signal and idler Poynting vectors generate tilted and dispersed signal and idler beams with large bandwidths. Further, injection seeding these devices requires unusual procedures. These effects can be eliminated by simple modifications of OPO design including walk-off compensation or image-reversing ring cavities. Because tilt and dispersion are associated with noncolinear signal and idler Poynting vectors, they are inherent to colinear type II OPO's and to noncolinear type I OPO's. However, with proper pump tilts, they can be eliminated in noncolinear type II OPO's. We find that injection seeding devices without tilt is straightforward, with no frequency shifts or tilts of the output light. Finally, although we did not discuss it, we find that there is relatively little difference in pump threshold or conversion efficiency among the designs covered in this paper.

ACKNOWLEDGMENTS

This work was supported by the United States Department of Energy under contract DE-AC04-94AL85000. Sandia is a multiprogram laboratory operated by Sandia Corporation, a Lockheed Martin Company, for the United States Department of Energy.

REFERENCES

1. A. V. Smith and M. S. Bowers, "Phase distortions in sum- and difference-frequency mixing in crystals," J. Opt. Soc. Am. B **12**, 49-57 (1995).

2. J. G. Haub, R. M. Hentschel, M. J. Johnson, and B. J. Orr, "Controlling the performance of a pulsed optical parametric oscillator: a survey of techniques and spectroscopic applications," J. Opt. Soc. Am. B **12**, 2128-2141 (1995).

3. J. G. Haub, M. J. Johnson, A. J. Powell, and B. J. Orr, "Bandwidth characteristics of a pulsed optical parametric oscillator: application to degenerate four-wave mixing spectroscopy," Opt. Lett. **20**, 1637-1639 (1995).

4. Y. R. Shen, The principles of nonlinear optics Wiley & Sons, New York, 1984.

5. Gunnar Arisholm, "Advanced numerical simulation models for second-order nonlinear interactions" , Proc. SPIE vol. 3685 Laser Optics '98: Fundamental Problems of Laser Optics, N. N. Rozanov editor

6. Gunnar Arisholm, "Quantum noise initiation and macroscopic fluctuations in optical parametric oscillators," to be published in J. Opt. Soc. Am. B., January 1999.

7. A. V. Smith, W. J. Alford, T. D. Raymond, and M. S. Bowers, "Comparison of a numerical model with measured performance of a seeded, nanosecond KTP optical parametric oscillator," J. Opt. Soc. Am. **12**, 2253-2267 (1995).

8. A. V. Smith, Russell J. Gehr, and Mark S. Bowers, "Numerical models of broad-bandwidth nanosecond optical parametric oscillators," submitted to JOSA B.

9. H. Vanherzeele, J. D. Bierlein, and F. Zumsteg, "Index of refraction measurements and parametric generation in hydrothermally grown $KTiOPO_4$", Appl. Opt. **27**, 3314 (1988).

10. R. Danielius, A. Piskarskas, P. Di Trapani, A. Andreoni, C. Solcia, and P. Foggi, "A colinearly phase-matched parametric generator/amplifier of visible femtosecond pulses,"

IEEE J. Quant. Electron. **34,** 459-463 (1998).

11. B. A. Richman, S. E. Bisson, R. Trebino, E. Sidick, and A. Jacobson, "Efficient broad-band second-harmonic generation by dispersive achromatic nonlinear conversion using only prisms," Opt. Lett. **23,** 497-499 (1998).

12. This case was modeled using function 2Dmix-SP in the SNLO software package which is freely distributed at http://www.sandia.gov/imrl/XWEB1128/xxtal.htm.

13. M. J. T. Milton, T. J. McIlveen, D. C. Hanna, and P. T. Woods, "High-efficiency infrared generation by difference-frequency mixing using tangential phase matching," Opt. Comm. **87,** 273-277 (1992).

14. G. C. Bhar, U. Chatterjee, and S. Das, "Tunable near-infrared radiation by difference frequency mixing in beta barium borate crystal," Appl. Phys. Lett. **58,** 231-233 (1991).

15. T. D. Raymond, W. J. Alford, A. V. Smith, and M. S. Bowers, "Frequency shifts in injection-seeded optical parametric oscillators with phase mismatch," Opt. Lett. **19,** 1520-1522 (1994).

FIGURES

Fig. 1. The test OPO uses a 10 mm long, type II phase matched KTP crystal (cut at $\theta = 58°, \phi = 0°$) pumped by a 10 ns (FWHM), 532 nm, 0.65 mm diameter (FWHM irradiance), single-longitudinal-mode pulse. The physical cavity length is 12 mm, the pump and 1655.1 nm idler mirror reflectivities are zero, and the 784 nm signal mirror reflectivities are 1.0 and 0.71. The signal walk-off angle is 48.7 mrad; d_{eff} is 3.0 pm/V; signal/idler/pump refractive indexes are 1.816/1.735/1.790; the signal/idler/pump group velocity indexes are 1.876/1.765/1.911; the phase matching angle is θ=57°, ϕ=0°.

Fig. 2. (a) The beam path assumed by the signal wave in the monochromatic, phase matched OPO and (b) the signal beam path for the highest gain mode of operation. The dashed lines represent the walk-off path for an *e*-polarized beam with propagation vector along the cavity axis. The Δk's are for colinear propagation vectors. Note that the tilt angles are greatly exaggerated in these diagrams. The actual beam tilts of about 5 mrad are much smaller than the walk-off angle of about 50 mrad.

Fig. 3. (a) Model-generated contour plots of signal energy fluence for the test OPO versus angle relative to the cavity axis on the horizontal axis and detuning from the phase matched wavelength on the vertical axis. The dashed line shows the calculated phase matching frequency versus crystal angle. (b) Far-field signal energy fluence contours.

Fig. 4. Laboratory apparatus for characterizing KTP OPO's. Details are given in the text.

Fig. 5. (a) Measured contour plots of signal energy fluence for the test OPO versus angle relative to the cavity axis on the horizontal axis, and detuning from the phase matched wavelength on the vertical axis. (b) Far-field signal energy fluence contours.

Fig. 6. Diagram of noncolinear phase matching for a pump beam propagating at angle θ_p relative to the crystal optic axis z. S_s is the signal Poynting vector tilted by angle ρ_s relative to the signal propagation vector k_s. The Poynting vector makes an angle of α with respect to the optic axis.

Fig. 7. (a) Diagram of parametric amplification of small diameter, short duration signal/idler pulse by larger, longer pump pulse illustrating the origin of tilted structure in the amplified signal and idler waves. The ellipses represent half-height contours of irradiance for the input pump, signal, and idler in the left diagram. In the right diagram, the dashed lines show the paths (in reference frame moving with the pump pulse) that would be followed by the input signal and idler pulses during linear propagation through the crystal. Due to the combination of group velocity and birefringent walk-off relative to the pump the input signal and idler pulses trace the lower and upper dashed lines respectively. The signal and idler light generated in the crystal fill in the tilted slanted connecting the signal and idler end points. (b) Equivalent slanted pulses can be created by reflecting a short, unslanted signal pulse off a diffraction grating.

Fig. 8. (a) Measured signal dispersion diagrams showing partial seeding for crystal tilted to shift free running wavelength toward the seed wavelength, and (b) the corresponding far-field signal fluence profile.

TABLES

Table 1. Model results for 12 mm long cavity with 10 mm crystal and 6 mJ pump.

Configuration	*e* waves	Resonated wave	Signal tilt (mrad)	Shift (GHz)	Bandwidth (GHz)	Dispersion (μrad/GHz)
SW	i	i	2.2	360	66	6.1
SW	i	s	3.4	550	133	6.2
SW	s	i	-1.8	310	140	-5.7
SW	s	s	-3.2	570	300	-5.7
SW	p	s	0.16	0	60	
SW	none	s	0	0	40	
SW	s,i	s	-0.5	0	60	
ring	s	s	0	0	25	
WOC-SW	s	s	0	0	35	

Table 2. Signal tilt for different cavity lengths with 10 mm crystal.

Cavity length (mm)	Measured signal tilt (mrad)	Calculated signal tilt (mrad)	Measured pump threshold (mJ)
12.0	6.6	3.3-3.9	3.1
12.5	6.1		3.35
14.0	5.3		3.4
15.0		2.4-2.6	
16.0	4.7		3.65
17.5	4.4		4.0
20.0	4.0	1.7-2.1	

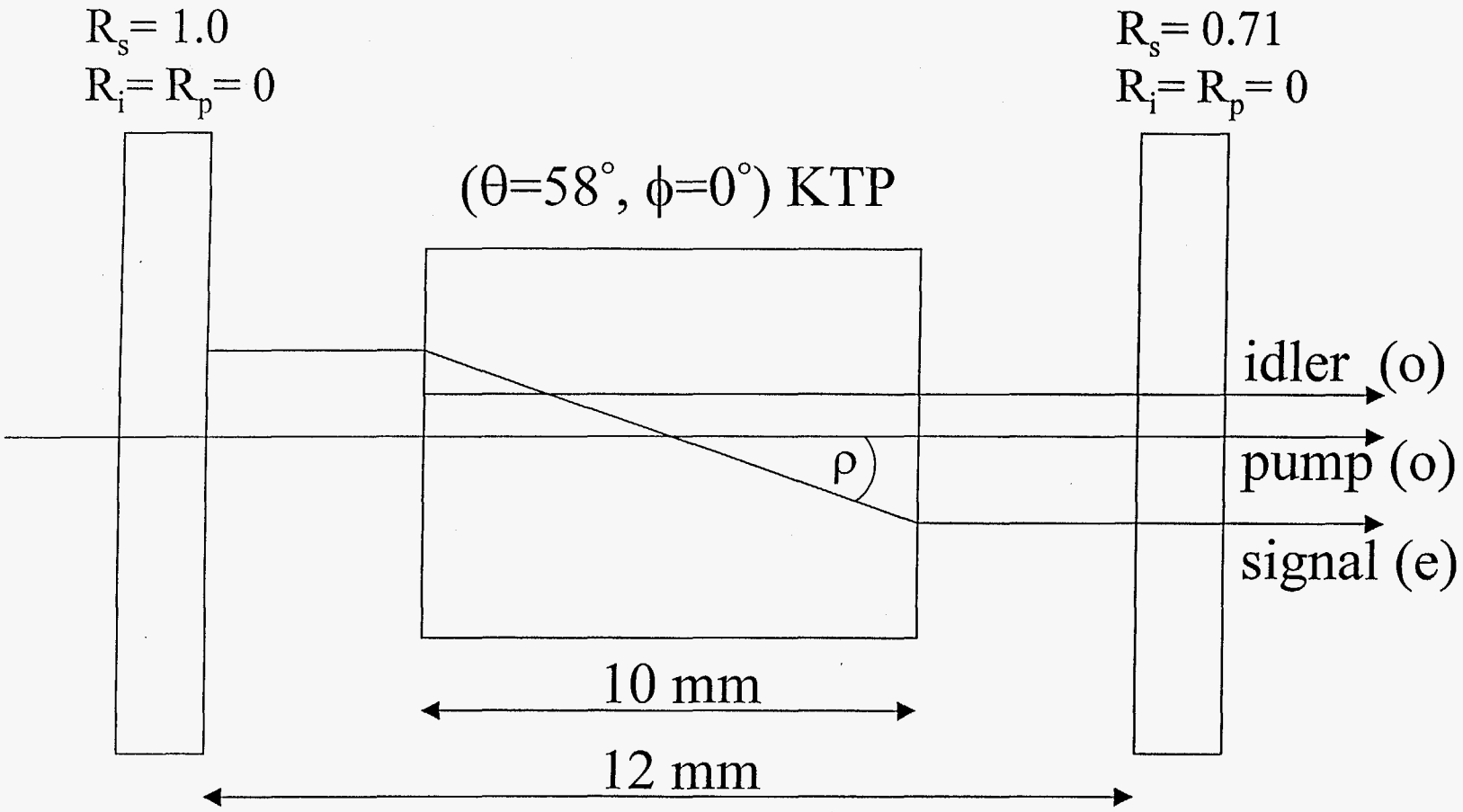
R_s= 1.0
R_i= R_p= 0
R_s= 0.71
R_i= R_p= 0
(θ=58°, ϕ=0°) KTP
idler (o)
pump (o)
signal (e)
ρ
10 mm
12 mm

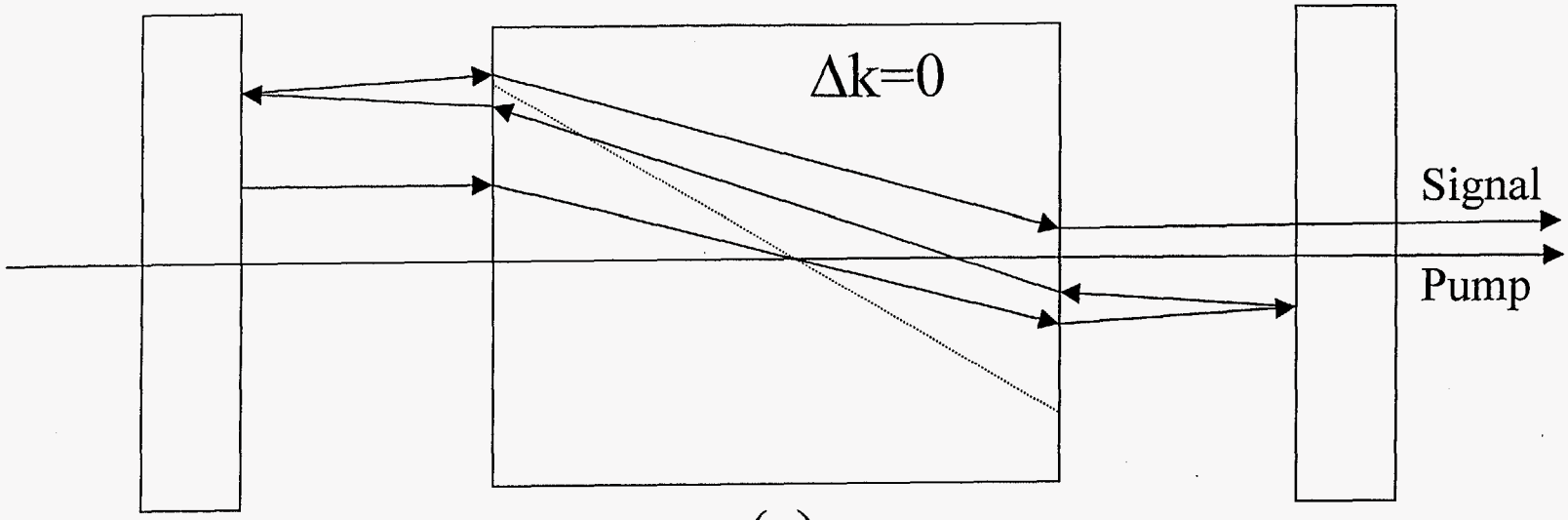

(a)

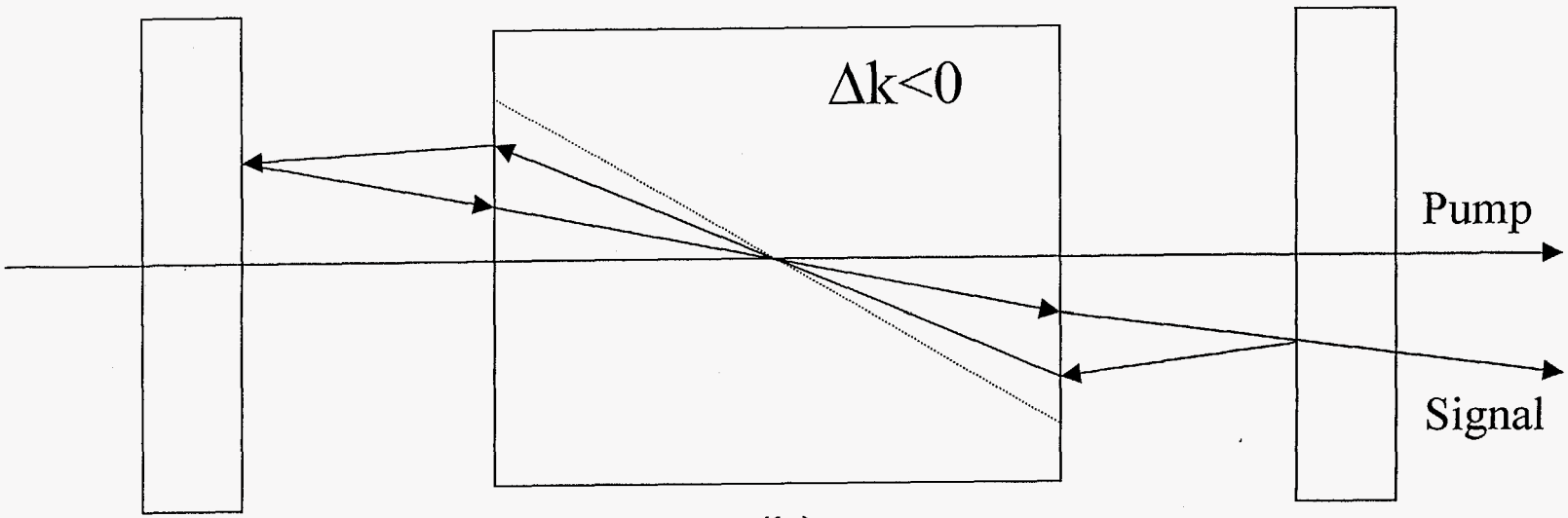

(b)

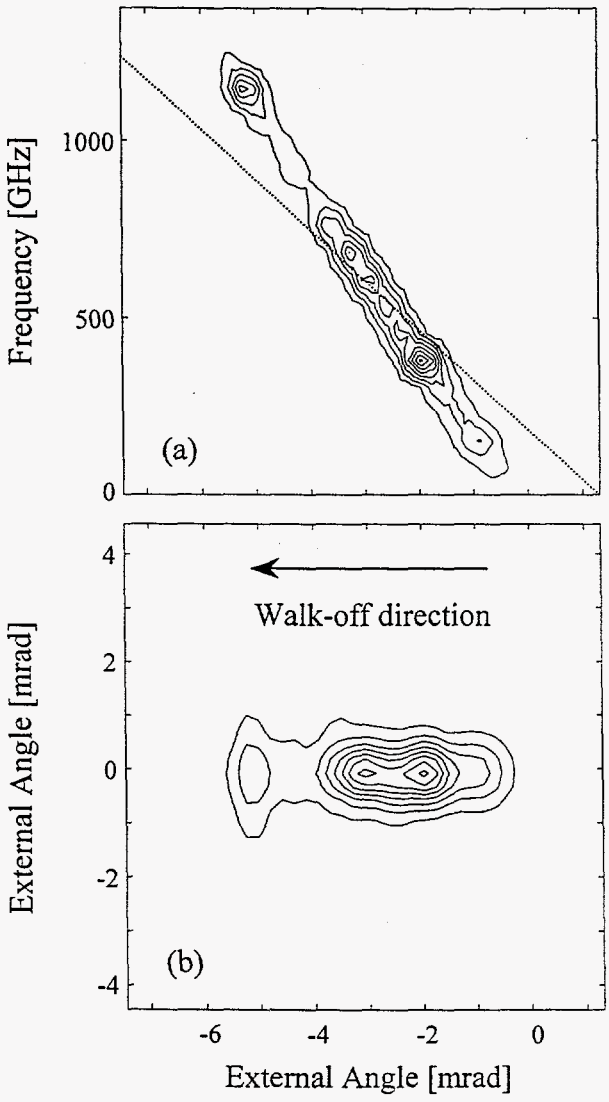
Frequency [GHz]
1000
500
0
(a)
External Angle [mrad]
4
2
0
-2
-4
Walk-off direction
(b)
-6
-4
-2
0
External Angle [mrad]

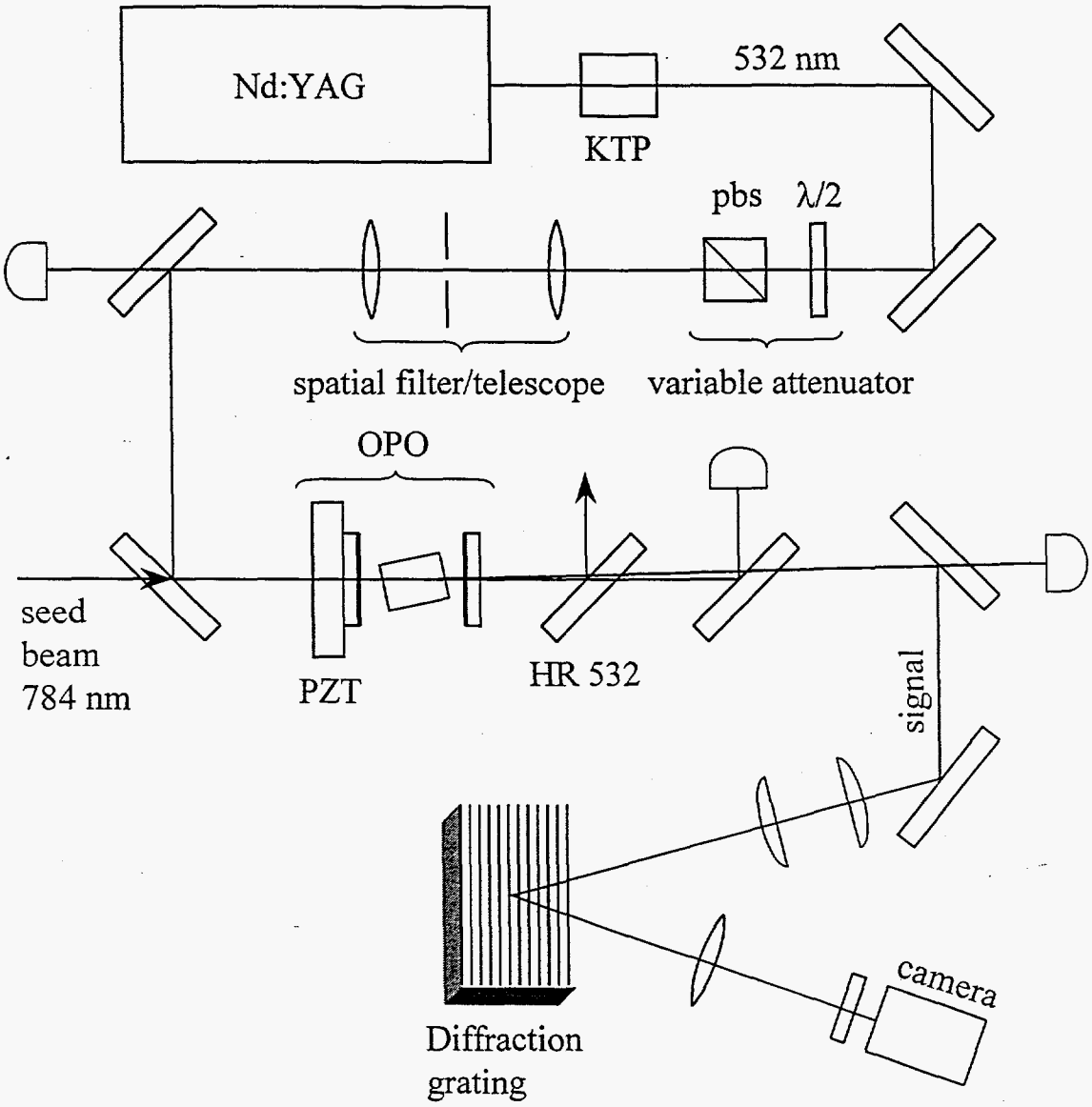
Nd:YAG
532 nm
KTP
pbs
λ/2
spatial filter/telescope
variable attenuator
OPO
seed
beam
784 nm
PZT
HR 532
signal
camera
Diffraction
grating

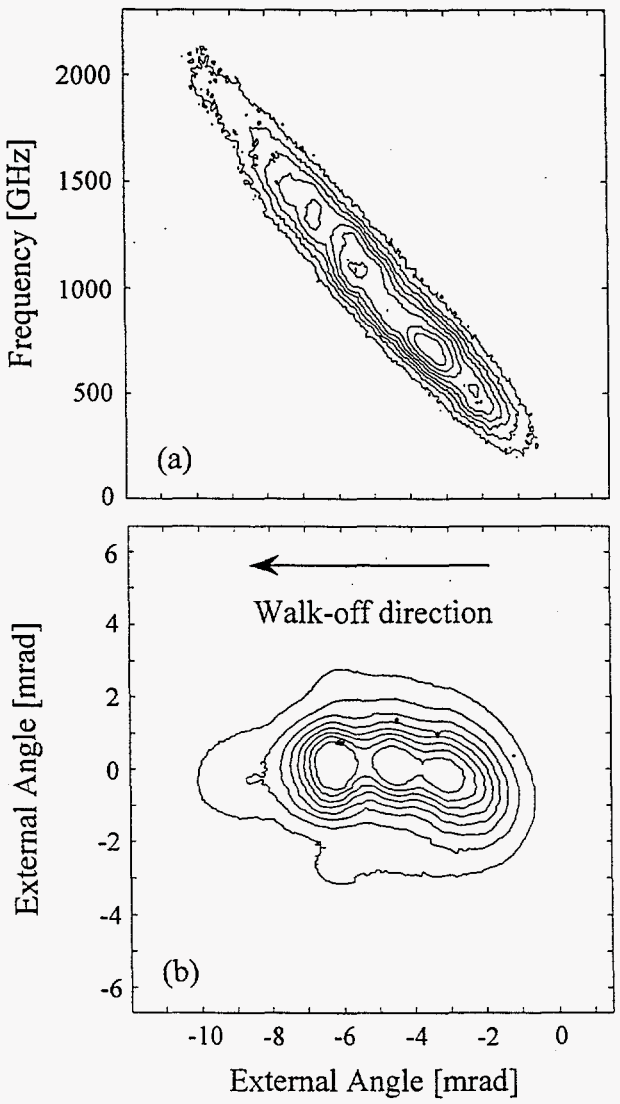
Frequency [GHz]
2000
1500
1000
500
0
(a)
Walk-off direction
External Angle [mrad]
6
4
2
0
-2
-4
-6
(b)
-10
-8
-6
-4
-2
0
External Angle [mrad]

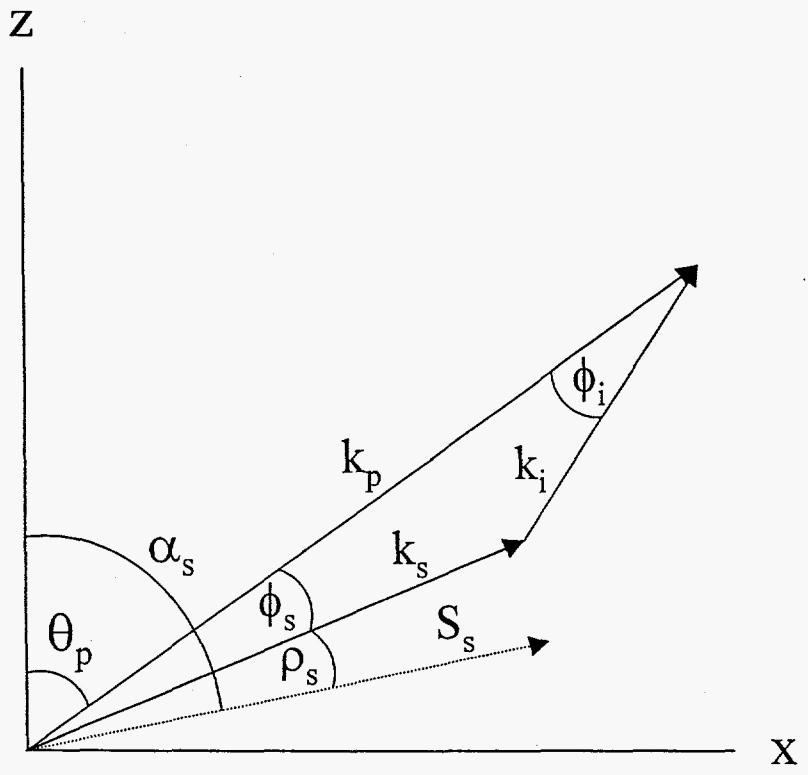
z
x
ϕ_i
k_p
k_i
α_s
k_s
ϕ_s
θ_p
S_s
ρ_s

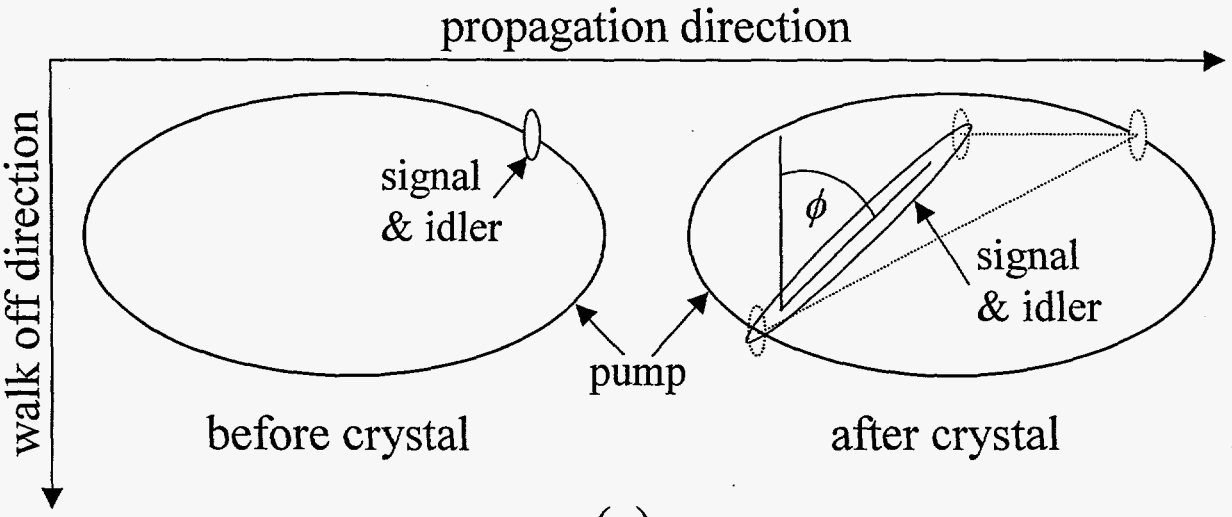
propagation direction
walk off direction
signal
& idler
pump
signal
& idler
before crystal
after crystal

(a)

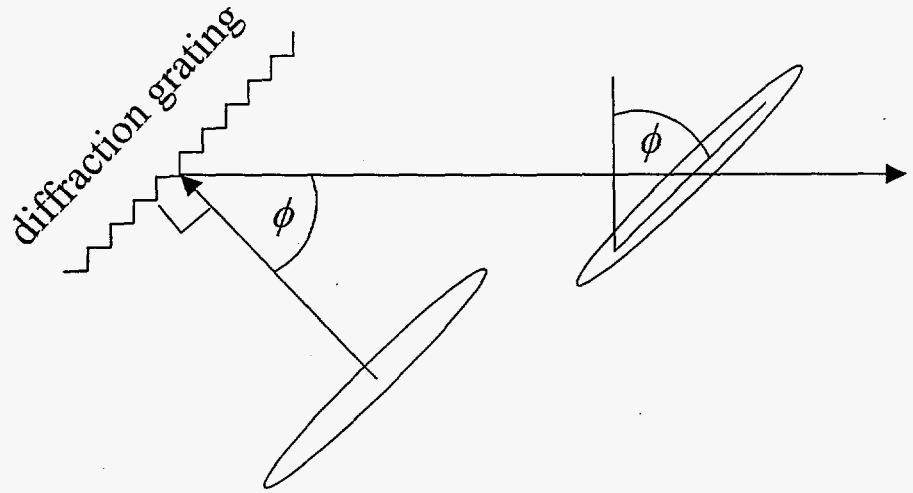
diffraction grating

(b)

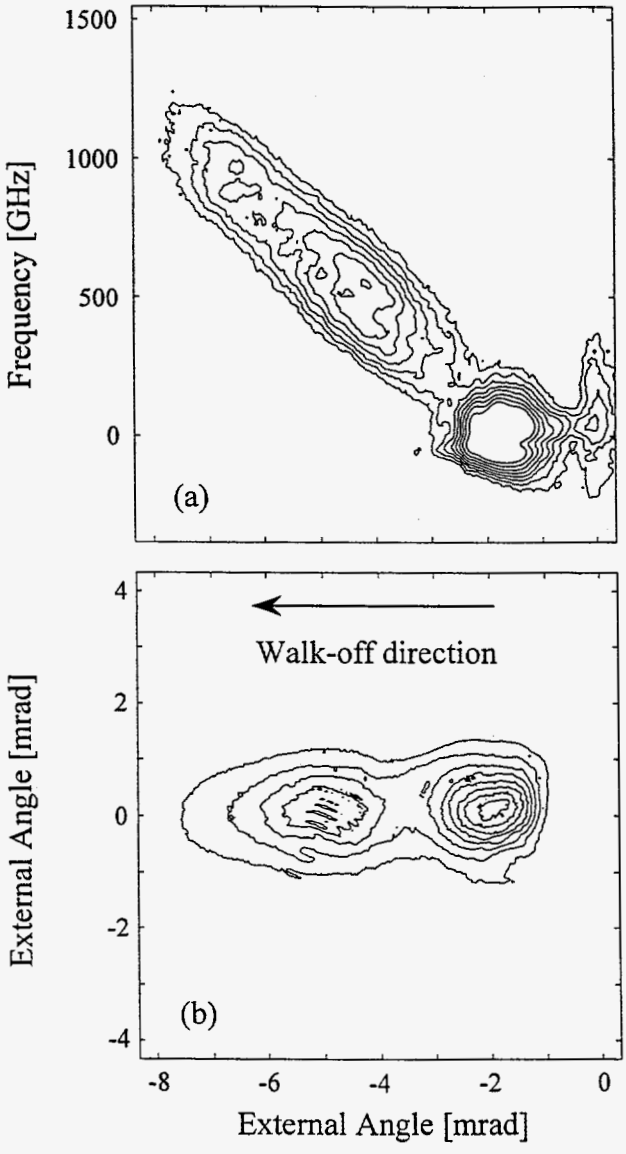
1500
1000
500
0
Frequency [GHz]
(a)
4
2
0
-2
-4
External Angle [mrad]
Walk-off direction
(b)
-8
-6
-4
-2
0
External Angle [mrad]